Transverse Beam Profile Analysis of a Plasma Sputter Ion Source

Alexander Mendenilla, Carlo Mar Blanca, and Henry Ramos*
National Institute of Physics, College of Science
University of the Philippines, Diliman, Quezon City 1101
E-mail: hramos@nip.upd.edu.ph

ABSTRACT

The beam profile of an existing plasma-sputter-type negative ion source with a titanium target is analyzed. The transverse characteristics of the ion beam are investigated and the deposition capability of the system is characterized. The ambient plasma parameters are derived via a Langmuir probe indicating an electronic density of 9.2×10^{10} cm^{-3} and temperature of 2.14×10^4 K near the center of the ion beam. Simulated negative ion distributions show that the energy content of the deposition plasma is three orders of magnitude lower than the expected current amplitude–the apparent effect of beam defocus. Although attenuation of the incident beam is apparent, the beam is basically monoenergetic, with a maximum energy spread of 8eV.

INTRODUCTION

It has long been recognized that surface coatings offer increased opportunity to select materials most appropriate in providing excellent resistance to corrosion, wear, fatigue, and friction (Bunshah, 1982; Walther et al., 1990). Lately, there is notable interest in titanium ion Ti deposition because of its remarkable durability, making it important as a coating material on tools to extend their lifetime (Jiang et al.,1995; Scardi et al., 1991). Titanium films prepared on silicon have also been used as diffusion barriers for very large scale integrated (VLSI) circuits and as wear-resistant ceramic coatings (Sundgren et al., 1985).

So far, many coating techniques, such as chemical vapor deposition (CVD), physical vapor deposition (PVD) and ion plating, have been used to prepare Ti^- layers (Kajioka et al., 1996; Ahmed, 1994; Kadlee et al., 1989). However, films produced by these conventional techniques often exhibit poor adhesion to the substrates. A significant trend that has been used is the ion-beam-assisted deposition techniques in growing surface layers. It has shown significant advantages because of the freedom with which materials can be modified by adjusting the ion current or energy of an independent ion beam. This method has improved adhesion to the substrate and enabled growing films at low temperature by the aid of energetic ions (Rossnagel and Cuomo, 1987; Smidt, 1990). Thus, ion beam-assisted deposition has become an effective means of growing high-quality films.

A major detriment to this deposition process is the low-electron affinity of Ti^-, which poses a formidable problem in ion coating because a significant magnitude of the plasma flux is mandatory for proper deposition. Therefore, there is a need for appropriate beam characterization as functions of the various plasma operating parameters. The critical dependence of the application on the amount of impurities and on strict energy requirements constrain us to develop a technique to investigate the depository beam. In particular, we investigate the transverse energy density characteristics of the Ti^- ions and evaluate whether the ion flux is high enough to achieve proper deposition. This is implemented using an electrostatic energy analyzer

Key words: plasma physics, film deposition

**Corresponding author*

(ESA) with a typical current density of 0.25 nA/mm^2. The ESA is interfaced to a computer via a GPIB driver to permit the rapid and accurate determination of the energy density. The dependence of the beam characteristics on the operating conditions (electron temperature, density and plasma space potential) is investigated via a Langmuir probe. The plasma source geometry is described in Sec. II and the experimental results are given in Sec. III. The feasibility of the facility for ion deposition is then evaluated in the last section.

METHODOLOGY

A layout of the facility is shown in Fig. 1. The left side of the whole system is the plasma production chamber, while the right end of the facility is the deposition chamber. The connecting chamber houses the diagnostic system for the ion beam source (Okabe et al., 1991). The Ti target is connected to a water-cooled copper electrode, which is biased negatively with respect to the plasma. The energy provided by the potential difference accelerates the positive ions across the plasma sheath and into the Ti target. Ti^- ions are then produced and self-extracted into the diagnostic system.

A turbo molecular pump backed by a rotary pump evacuates the ion production chamber and it normally attains a base pressure of 5.0 x 10^{-6} Torr. The oxygen/ argon plasma is produced at initial gas filling pressures of 3.15 x 10^{-5} Torr O_2 and 6.7 x 10^{-3} Torr argon. Operating parameters for the discharge are discharge current (I_d)= -0.8A, discharge voltage (V_d)= -40V, target voltage (V_t)= -200V, target current (I_t)= -30 mA and filament current (I_f)= 8.5A. It is at these settings that quiescent plasma was achieved. Discharge and target currents fluctuates to a minimum at these settings.

After the ignition of the plasma, a Langmuir probe trace is taken so as to determine critical parameters of the discharge such as the electron density, electron temperature and the plasma potential. The Langmuir probe setup can be seen in Fig. 2, which shows that the tip of the probe is located at the center of the plasma. Subsequently, the energy spectrum is determined using a retarding potential-type ESA (Fig. 3) which is located inside the connecting chamber. A retractable bellows-type feedthrough is connected to the ESA so that the longitudinal energy spectrum can be determined. Data gathering from the Langmuir probe and the ESA is simplified by interfacing the data acquisition instruments

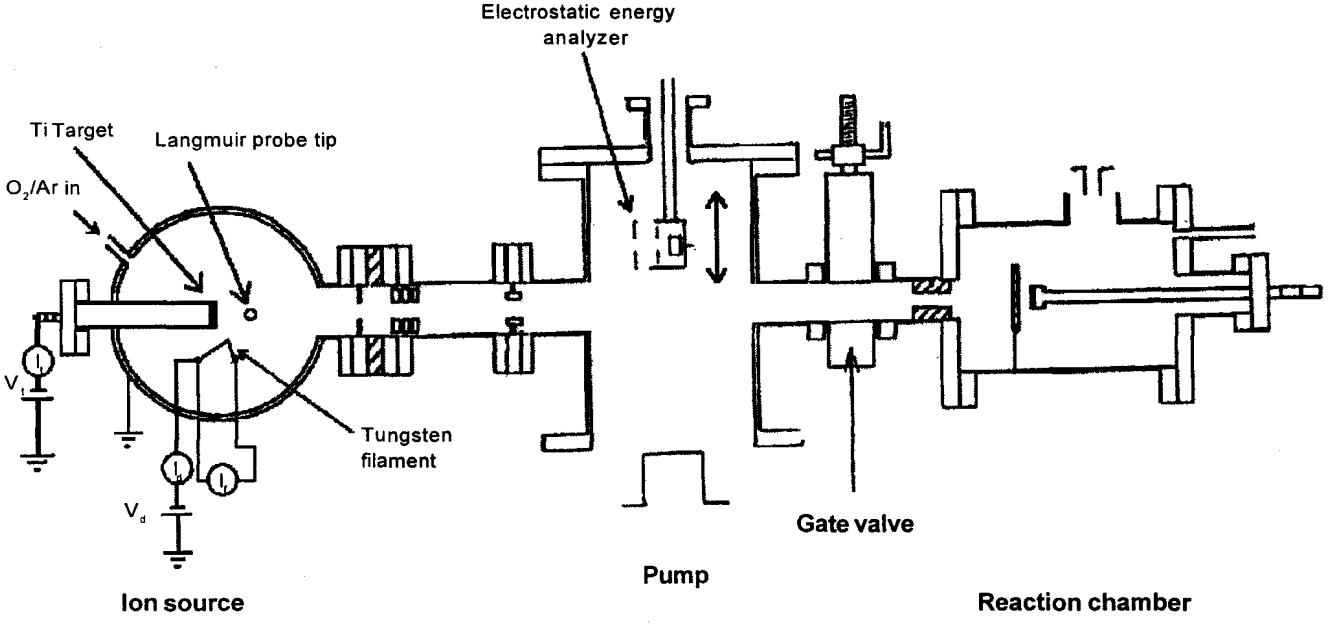

Fig. 1. Schematic diagram of the experimental set-up. The Langmuir probe is found inside the ion production chamber while the ESA is located inside the connecting chamber.

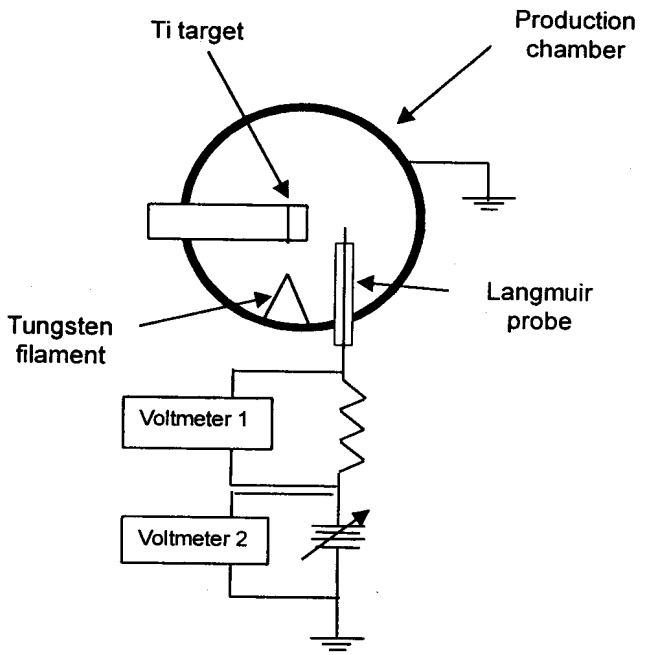

Fig. 2. Top cross section view of the production chamber including the connection setup for the Langmuir probe.

into an Intel-based computer via the general programmable interface bus (GPIB) protocol. The GPIB protocol has an advantage over most computer interface systems since the GPIB computer interface card does not introduce digital noise unlike normal analog-to-digital interface cards. The software is written in visual C++ so as to simplify the user-interface. The results are then recorded for data processing and analysis after the experiment.

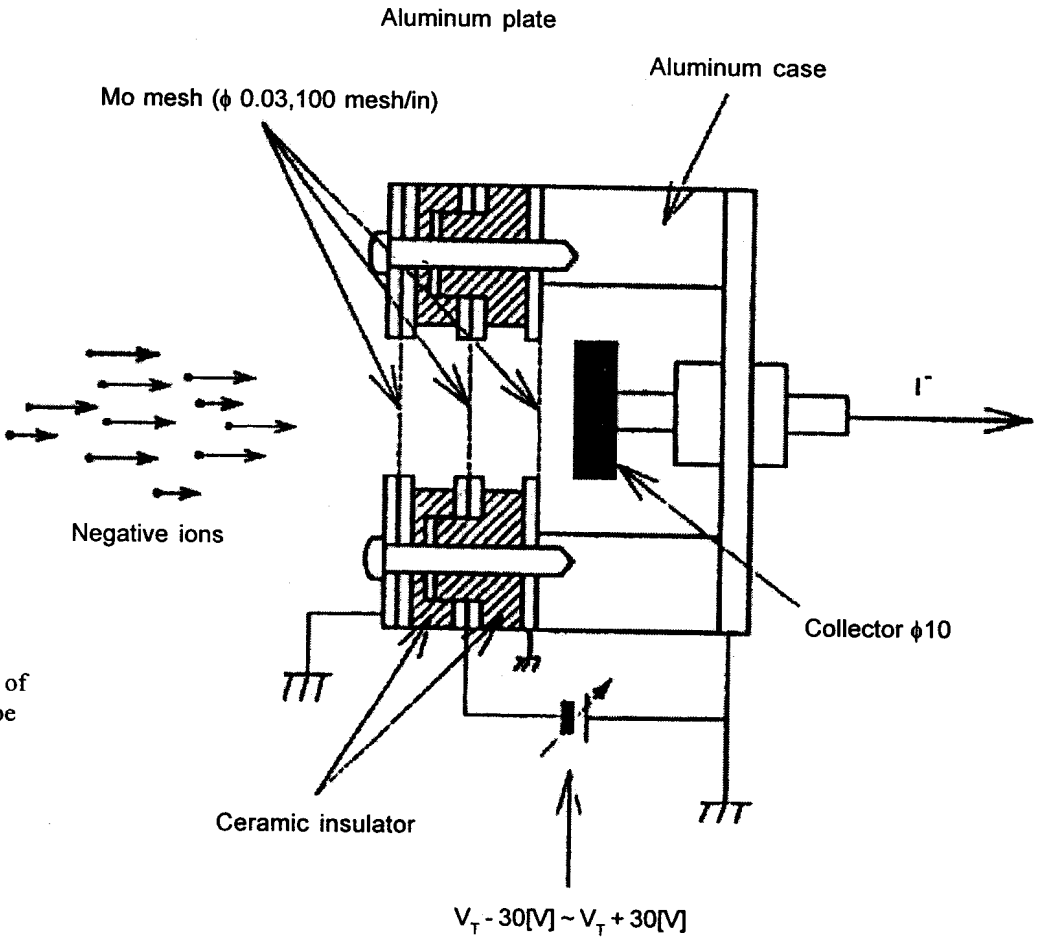

Fig. 3. Schematic diagram of the retarding potential-type energy analyzer.

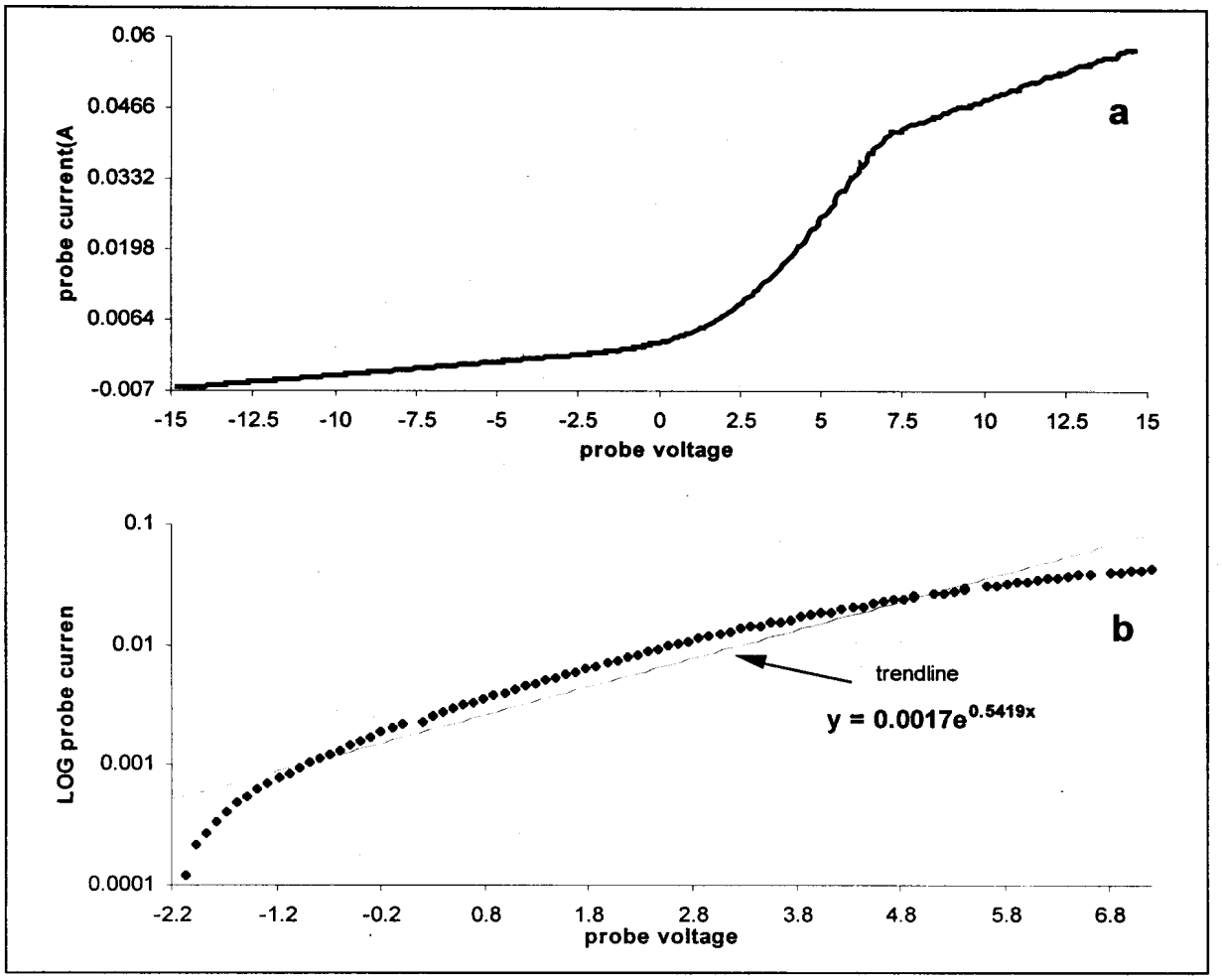

Fig. 4(a). Averaged Langmuir trace; (b) Log plot of the transition region. Operating parameters for the discharge are discharge current = -0.8A, discharge voltage = -40V, target voltage = -200V, target current = -30 mA and filament currrent = 8.5A.

RESULTS AND DISCUSSION

Langmuir probe measurements

A sample Langmuir trace is obtained and shown in Fig. 4a. The pertinent ambient parameters can then be derived from this particular trace. In the absence of any other external field sources, the electron distribution is primarily Maxwellian (Huddlestone and Leonard, 1965).

The region of concern for the determination of the electron temperature T_e occurs in the transition region, where the electron accelerates and builds up in the Langmuir probe producing the rising current. The shape of the transition curve of the Langmuir trace is related to the distribution of electron energies and hence gives the parameter T_e. Since the distribution follows a Maxwellian profile, the sloping rise is exponential in nature. Taking the variation of the logarithm of the current as a function of the voltage (Fig. 4b), the slope is directly proportional to the Maxwellian exponential power $|e/kT_e|$ where e is the electron charge and k is Boltzmann's constant. Linear regression analysis yields the log equation $y = 0.0017e^{0.5419x}$ and the computed electron temperature is $T_e = 2.14 \times 10^4$ K. The magnitude of the saturation electron current is a measure of $n(kT_e)^{1/2}$, from which the electron density

$n = 9.2 \times 10^{10}$ cm^{-3} is determined. These values fall within the range of typical of glow discharge plasmas (Garcia 1997).

The plasma potential is derived via extrapolation of the saturation and transition regions. The calculated plasma space potential is 6.8 volts. The strong positive value of the plasma space potential implies that both electrons and negative titanium ions are confined within the plasma which could result in a relatively high ion density being extracted and detected.

When the probe is sufficiently negative, only ions can reach the probe surface. Since the motion of the ions are not significantly affected by the potential across the sheath due to their masses, the ions are expected to reach the probe surface at their random thermal speed. This means that the rate of the number of ions reaching the probe is independent of the probe potential as long as it is sufficiently negative. This contributes to the ion saturation current which is a result of the random thermal motions of the ions and is given by

$$I_{ri} = 0.4 A e n_i \left(\frac{2kT_e}{m_i} \right)^{1/2} \quad (1)$$

where A is the effective probe area, e is the electron charge, n_i is the ion density and T_e is the electron temperature, k is the Boltzmann constant and m_i is the ion mass.

The electron random current gives the current contributed by the electron flow

$$I_{re} = A e n_e \left(\frac{kT_e}{2\pi m_e} \right)^{1/2} \quad (2)$$

The calculated current values are $I_{ri}=3.25 \times 10^{-6}$ A and $I_{re}=1.92 \times 10^{-3}$ A. These readings, too are valid within an order of magnitude to derived results (Garcia, 1997).

ESA traces

A retarding-potential type ESA interfaced via a GPIB bus is utilized to derive the transverse energy profile of the confined plasma. The various ESA traces at different transverse displacements Z are presented in Fig. 5. The value of Z is minimum at the base of the chamber and increases as the probe is scanned up the chamber's diameter. It is evident that the ESA provides detectable response only within the 20–40 mm range. The plots of the maximum detected current as a function of transverse displacement Z are given in Fig. 6. The current full-width-at-half-maximum (FWHM) occurs within the 15-40 mm range. Beyond this diameter, very low current value is obtained. This plot presents a qualitative profile of the distribution of the intensity of the plasma beam along its cross-section. For deposition applications where the target substrate has a surface area of 1 cm^2, this cross-section is large and may severely deplete the incident beam of its intensity because intensity varies inversely with illuminated area. If not focused properly, the target substrate can be swamped by the incident ions and deposition efficiency will be severely compromised.

As the plasma propagate along the length of the chamber, a significant broadening of the angular distribution of the sputtered species is encountered. This defocusing effect is caused by the large angular extent of the target, the initial cosine-like sputter emission distribution (Huddlestone and Leonard, 1965) and the collision broadening of this distribution (Backhouse et al., 1996).

The energy distribution of the Ti^- ions from a plasma sputter source is described by (Ramos et al., 1989; Ramos et al., 1990; Alton, 1989)

$$Y^- = 2\pi \int_0^{\pi/2} f(E,\theta) \eta^-(E,\theta) \sin\theta d\theta \quad (3)$$

where the energy distribution of particles ejected by sputtering is described by the Thomson relation (Thomson, 1968).

$$f(E,\theta) = \frac{2E_b}{\pi} \frac{E}{(E+E_b)^3} \cos\theta \quad (4)$$

Eb=4.85 eV is the surface binding energy of the particle to the solid. The negative ion production probability is (Ishikawa, 1988).

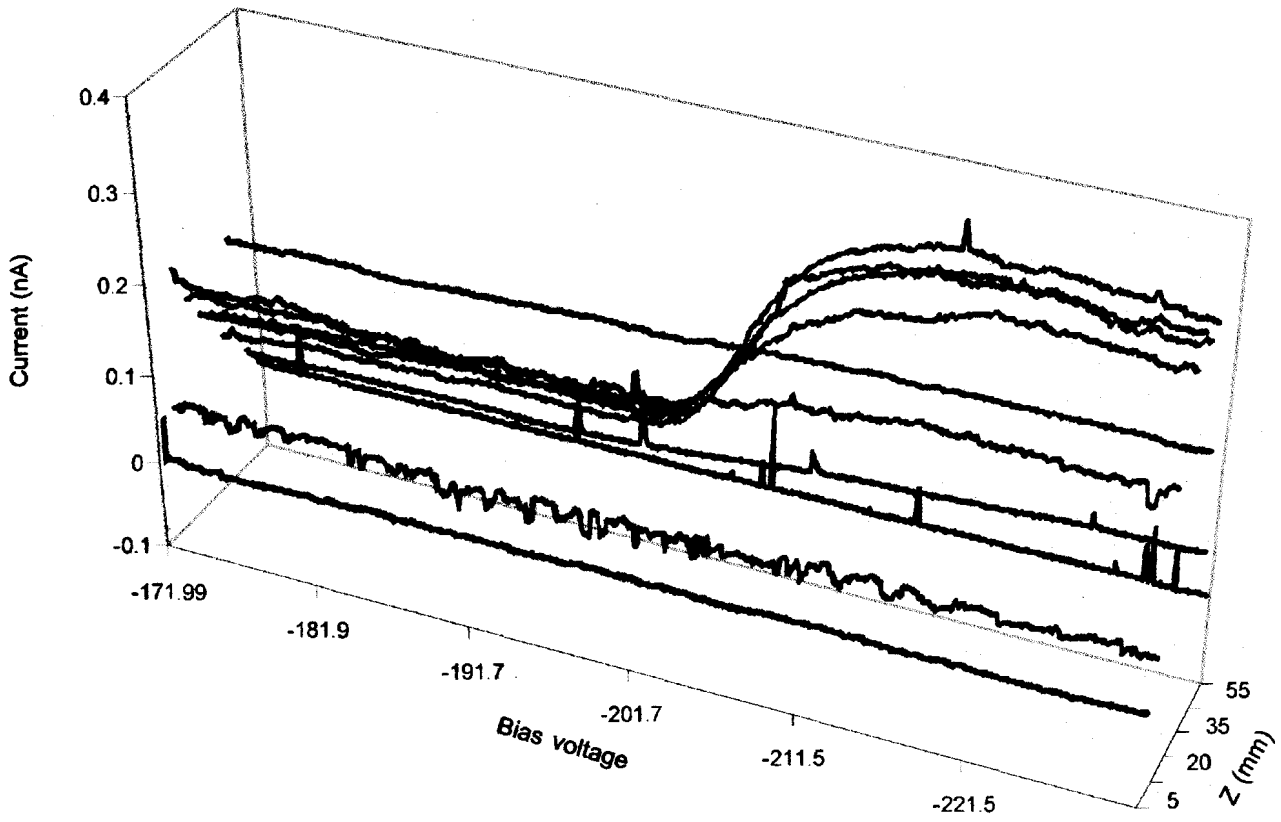

Fig. 5. ESA traces for different longitudinal displacements Z. Operating parameters for the discharge are discharge current = -0.8A, discharge voltage = -40V, target voltage = -200V, target current = -30mA, and filament current = 8.5A.

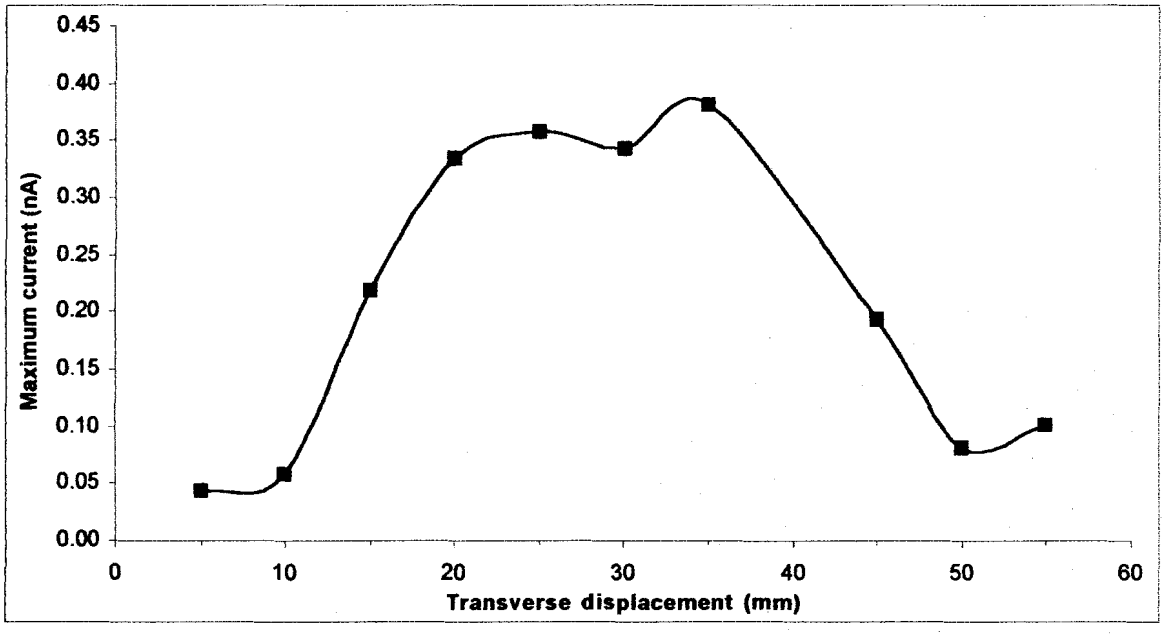

Fig. 6. Plot of maximum ESA current for different transverse displacements. Operating parameters for the discharge are discharge current = -0.8A, discharge voltage = -40V, target voltage = -200V, target current = -30 mA, and filament current = 8.5A.

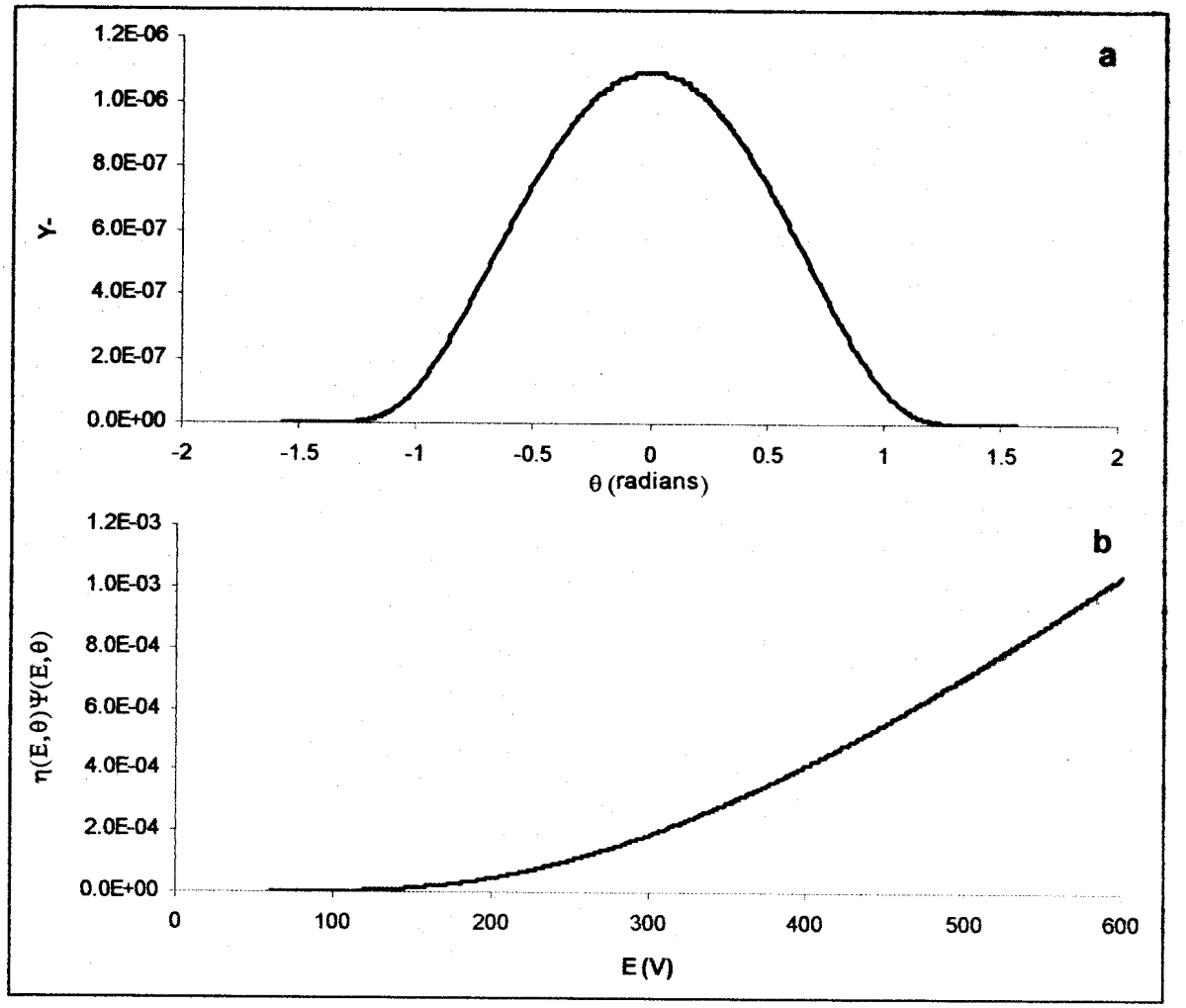

Fig. 7. (a) Plot of the energy distribution Y^- as a function of the ejection angle ($-p/2 \leq q \leq p/2$) for E=200 V. This gaussian curve concentrates most of the ions near the propagation axis of the chamber but broadens with propagation. **(b)** Plot of the h(E,q)Y(E,q) as a function of E.

$$\eta^-(E,\theta) = \frac{2}{\pi}\exp\left[\frac{(\phi - E_a)}{\gamma v_N / c}\right] \qquad (5)$$

where

$v_N = \sqrt{2E/M}\cos\theta$

$\gamma / c = 3 \times 10^{-7}$ eV cm^{-1}s

M = 47.9, mass of Ti

E_a = 0.2 eV, electron affinity

ϕ = 3.7 ~ 4.3 eV, Ti work function

The plot of Y^- as a function of the ejection angle ($-\pi/2 \leq \theta \leq \pi/2$) is presented in Fig. 7A for E=200 V. This gaussian curve concentrates most of the ions near the propagation axis of the chamber and is similar to and supports the results in Fig. 6.

Should the ESA be moved in the axial direction, it is possible to determine a cylindrical profile of the energy spectrum and hence the beam divergence can be quantitatively characterized. Many pertinent information can then be extracted from the data including the description of the energy requirements for respectable Ti^- deposition, the degree of defocus encountered by the beam and the three-dimensional distribution of the current, temperature and even electrical conductivity of the plasma. However, since the existing set-up is constrained to move only along

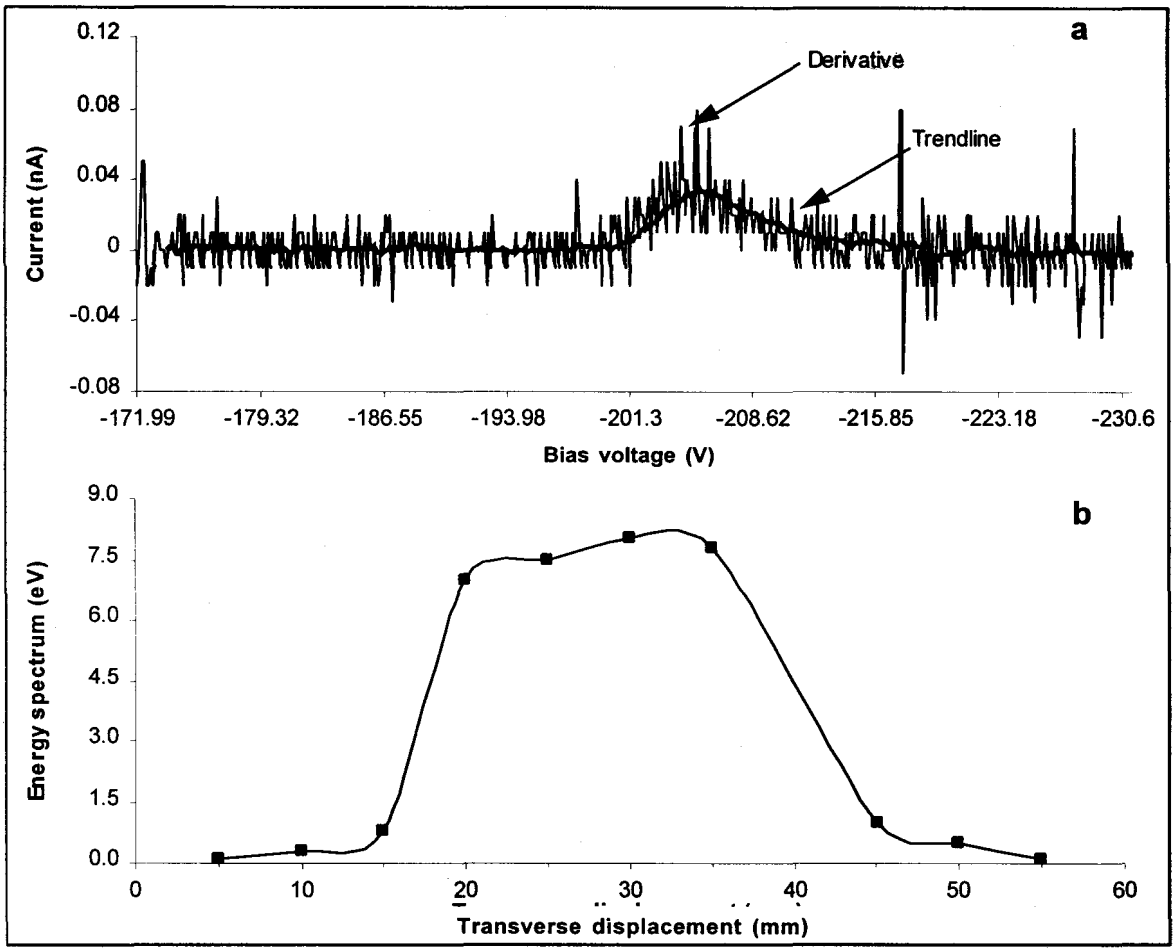

Fig. 8. **(a)** Representative plot of the derivative of the ESA trace for x = 35 cm. The solid line is the trendline obtained by the moving average protocol. **(b)** The FWHM of the energy spectrum for different x values. Operating parameters for the discharge are discharge current = -0.8A, discharge voltage = -40V, target voltage = -200V, target current = -30 mA and filament current = 8.5A.

the beam cross-section, numerical approximations shall be utilized as an alternative in gauging the deposition performance of the set-up.

The negative ion current can be obtained using the equation

$$I^- = \eta^- Y I^+ \tag{6}$$

where I^+ is the positive ion current for sputtering. The sputtering yield of the metal is (Matsunami et al., 1984)

$$Y = 0.42 \frac{\alpha Q K S_n(\varepsilon)}{\mu_s [1 + 0.35 \mu_s s_c(\varepsilon)]} \left[1 - \left(E_{th}/E\right)^{1/2}\right]^{2.8} \tag{7}$$

where

μ_s = 4.85 eV = sublimation energy
α = 0.194
Q = equal parameter
$S_n(\varepsilon)$ = stopping cross section
ε = reduced energy
E_{th} = threshold energy
E = energy

The simulated $\eta^- Y$'distribution is plotted in Fig. 7b as a function of voltage E. In order to derive the expected negative ion current, we multiply the value of this distribution at E = 200 V by the maximum random

current derived from the Langmuir. The maximum negative ion current drawn from the ESA plot is 0.143 nA which is three orders of magnitude less than the expected Ti^- ion current. This attenuation is due to the defocusing encountered by the beam.

Proper characterization of the transverse energy content of the plasma involves the determination of the energy spectrum per ESA trace. The energy spectrum of the plasma beam incident on the ESA can be calculated by taking the FWHM of the first derivative of the ESA current with the potential. The numerical differentiation algorithm employed makes use of the central difference approach (Matsunami et al., 1984).The resulting derivative plot in Fig. 8a is plagued with spurious noise due to numerical quantization. The noise is filtered out using the "moving averages" approach with a period of 20 (Excel Macro Options; MicroCal Origin) The resulting trendline is the solid line plot in Fig. 8a.

If the preceding approach is applied to the different SA readings in Fig. 5, it is possible to derive the behavior of the energy spectrum as a function of Z. The resulting cross-sectional distribution of the energy spectrum is plotted in Fig. 8b. The amplitude of the plot represents the degree of variation of the energy as a function of distance Z. The deviation of the order of magnitude is less when it is near the propagation axis than when it is far from the axis. Thus, near the beam center, the ions are not monoenergetic (the energy spread proportional to the spectrum amplitude of the plot). The ideal case is an equal energy spread for all displacements. But since the maximum spread derived from the plot is a mere 8 eV, the system can function as a monoenergetic ion source.

CONCLUSION

The transverse energy distribution of a Ti^- ion beam is investigated and the deposition capability of the system is characterized using a GPIB-controlled electrostatic energy analyzer (ESA). The plasma operational parameters are derived via a Langmuir probe indicating an electronic density of 9.2×10^{10} cm^{-3} and temperature of 2.14×10^4 K at the beam. Because of beam defocusing, the plasma source can only produce an energy spread of 8 eV. Compared with the accepted implantation energy requirement (10-400 keV) (Walther et al., 1990), the present set-up is inadequate for proper deposition. Future research entails the use of an electrostatic Einzel lens that focuses the divergent beam onto the target substantially increasing the Ti^- yield.

REFERENCES

Ahmed, N. A. G., 1994. Ion plating: optimum surface performance and material conservation. Thin Solid Films 241: 179-183.

Alton, G.D., 1989. "The sputter generation of negative ion beams," Nucl.Instrum.and Methods in Phys. Research 37 (38): 45-55.

Backhouse, C. J., K. Robbie, J. Parks, J. Broughton, S. Dew, G. Este, & M. Brett, 1996. Electrostatic scattering of ionic species in low pressure sputtering of Ti and TiN. J. Vac Sci Technol. 14: 2175.

Bunshah, R., 1982. Deposition Technology for films and coatings: development and applications. Noyes Publications, New Jersey, 83 pp.

Excel Macro Options, Microsoft Excel 97 SR-1, Copyright 1985-97 MicroSoft Corporation.

Garcia, A. F. "Design and Construction of a Computer-Controlled Data Acquisition System for Use on a Languir Probe." BS Thesis, University of the Philippines Diliman, 1997.

Huddlestone, R. H. & S.L. Leonard, 1965. Plasma Diagnostic Techniques, Academic Press, New York, 101 pp.

Ishikawa, J., 1988. Proc. Symp. On Negative Ion Sources and Their Applications In Y. Mori & A. Takagi (eds.) KEK Report 88-7 .

Jiang, H., H. K. Tao, & H. Li, 1995. Structure of TiNx($0<x<1.1$) films prepared by ion-beam assisted deposition. Thin Solid Films 258: 51-55.

Kadlee, S., J. Musil, & W. D. Münz, 1989. Sputtering systems

with magnetically enhanced ionization for ion plating of TiN films. J. Vac Sci Technol A, 8: 1318-1324.

Kajioka, H., K. Higuchi, & Y. Kawashimo, 1996. Optical emission spectroscopy from arc-like Ti vapor plasma and effects of self-ion bombardment on Ti and TiN film deposition. J. Vac Sci Technol. 14:3147-3155.

Matsunami, N., Y. Yamamura, Y. Itikawa, Y. Kazumata, S. Miyagawa, K. Morita, R. Shimizu & H. Tawara, 1984. Atomic and Nuclear Data Tables.

MicroCal Origin, Version 3.01, Copyright 1991-93 MicroCal Software Inc., One Roundhouse, North Hampton, USA.

Okabe, Y., M. Sasao, H. Yamaoka, M. Wada & J. Fujita, 1991. Dependent of Au-production upon the target work function in a plasma sputter-type negative ion source. Jpn. J. Appl. Phys. 30: 1307-1312.

Ramos, H. J., M. Sasao, H. Yamaoka, & M. Wada, 1989. Effect of converted electrode in a multicusp negative ion source. Institute of Plasma Physics Research Report IPPJ-914, Nagoya University, May 1989.

Ramos, H. J., A. Taniike, M. Sasao, & M. Wada, 1990. Development of ion source for high grade coatings. Paper presented during the 15th Annual conference of the Japan Society of Furion and Plasma Science Research, September 22-26, 1996, Osaka, Japan.

Rossnagel, S. & J. Cuomo, 1987. Low-temperature film growth using highly-energetic ions. MRS Bull. 6(40): 12-16.

Scardi, P., D. Kothari, & L. Guzman, 1991. X-ray diffraction peak profile analysis of TiNx films prepared on silicon by reactive ion beam assisted deposition. Thin Solid Films 195: 213-218.

Smidt, F. A.,1990. Use of ion beam assisted deposition to modify microstructure and properties of thin films. Int Mater Review 35: 61-128.

Sundgren, J., E. J. Birch & G. Hakansson, 1985. Growth, structural characterization and properties of hard and wear-protective layered materials. Thin Solid Films 193/194: 818: 821.

Thompson, M. W., 1968. Plasma ion sputter source. Philosophical Magazine 377: 21-28.

Walther, S. R., K. N. Leung, & W. Kunkei, 1990. Production of atomic nitrogen ion beams. Rev. Sci. Instrum. 61:315-317.